3-4-2 Relation between Equatorial Ionospheric Scintillations and Atmospheric Waves from Below

OGAWA Tadahiko

This paper reviews some results from equatorial GPS ionospheric scintillation observations that have been conducted at Kototabang, Indonesia since January 2003, and briefly discusses relations between scintillation and atmospheric waves from below. GPS scintillations caused by plasma bubbles appeared between 2000 and 0100 LT mainly in equinoctial months, and their activity decreased with decreasing solar activity. The scintillation activity can be related to tropospheric disturbances over the Indian Ocean to the west of Kototabang. Scintillation index fluctuates with periods of planetary waves, and similar periods are also found in Earth's brightness temperature variations. Numerical simulations to know behavior of neutral wind in the equatorial thermosphere indicate that planetary waves dissipate rapidly above about 125 km, and short-period atmospheric waves become predominant above 100 km. It is suggested that these atmospheric waves can contribute to the generation of plasma bubbles causing the scintillations.

Keywords
Equatorial ionospheric disturbance, Ionospheric scintillation, Plasma bubble, GPS, Atmospheric wave

1 Preface

Plasma bubbles—disturbances peculiar to the equatorial ionosphere during the nighttime—are generated through the Rayleigh-Taylor plasma instability. The well-known basic physical process and characteristics of bubble generation alone do not allow us to fully understand the electrodynamic process regarding bubbles and equator spread F (see [1]). The possibility of atmospheric gravity waves (hereafter AGW) propagating through the equatorial thermosphere for the generation of bubbles and spread F has already been pointed out (see [2]-[7]). Ogawa et al. [8][9] discovered a wavy structure of the electron density in the equatorial anomaly (containing bubbles inside) with an east-to-west scale of several hundred to 1,000 km. Moreover, planetary waves (hereafter PW) having periods longer than two days were found to modulate the equatorial mesosphere and thermosphere [10][11]. And given these findings, in addition to the physical quantities (e.g., electric field, conductivity, neutral wind) peculiar to the ionosphere and thermosphere, the roles of AGW and PW in the electrodynamic process of equatorial ionospheric disturbances cannot be ignored [12].

Within the bubbles and in the surrounding area are electron density irregularities with various spatial scales. The radio waves of geostationary and orbiting satellites passing through these irregularities consequently undergo scintillation. Aboveground scintillation observation conducted using the radio waves of numerous GPS satellites enables the continuous monitoring of bubbles regardless of the weather, and helps to further elucidate the bubble phenomenon.

This paper analyzes the GPS scintillation data accumulated over long periods and gives an overview of the reasons for the daily changes in bubble activity and the causes of initial weak plasma disturbances that develop into bubbles. Note that the contents presented here have already been published in the form of papers in several journals [8][9][13]. For details, please refer to those documents.

2 Observation results of GPS scintillation

2.1 How to observe GPS scintillation

The observation of ionospheric scintillation of radio waves (1.5754 GHz) emitted by GPS satellites orbiting at an altitude of about 20,000 km began in the latter half of January 2003 at Kototabang (latitude 0.20° S, longitude 100.32° E; geomagnetic latitude 10.36° S) located near the geographic equator in West Sumatra, Indonesia [9][13][14]. Figure 1 shows the location of Kototabang. Three GPS receivers separated by a distance of about 130 m are arranged in a triangular pattern, with the signal intensity of each receiver being recorded at a sampling frequency of 20 Hz. A correlation analysis of the temporal changes in signals from the three receivers makes it possible to determine the drift velocity and direction of electron density irregularities (with a spatial scale of about 350 m) in the ionospheric F layer, that is, the drift velocity and direction of the plasma bubbles that cause GPS scintillations [14].

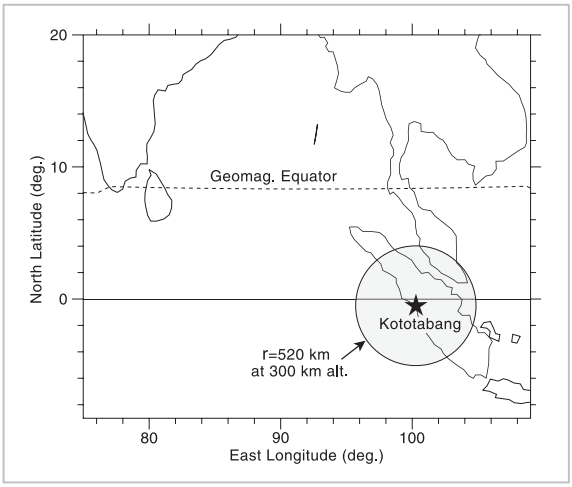

Fig.1 *Location (★) of Kototabang and the field of view for GPS scintillation observation*

(Satellite elevation angle ≥ 30° in a circle having a radius of 520 km centered at an altitude of 300 km right above Kototabang).

As an example, the bottom of Fig. 2 shows the temporal changes in GPS signal intensity received on April 1, 2003. The figure at the top shows a horizontal two-dimensional distribution of airglow photographed at 22:35 LT with a 630-nm all-sky camera; the several dark regions in thin long patterns extending south to north are plasma bubbles. At 22:15 to 22:40 LT, the signal intensity weakens and there are intense temporal changes in the intensity called scintillations. These scintillations occur when the radio wave propagation path between the GPS and ground passes through the plasma bubbles and proximity thereof having electron density irregularities. The bubble (marked with the white arrow) that developed as far as right above Kototabang caused the most intense scintillation at around 22:35 LT.

One indicator often used to represent scin-

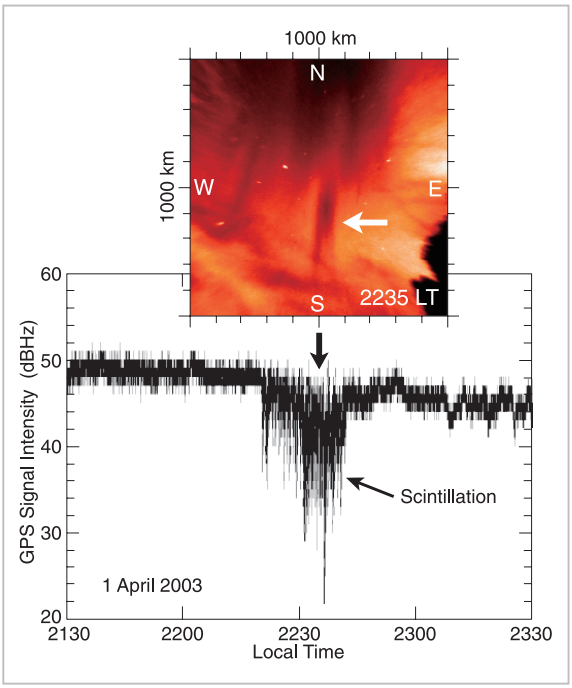

Fig.2 *GPS scintillations caused by plasma bubbles on April 1, 2003*

tillation intensity is an index called S_4. It is expressed as $S_4^2 = (\langle I^2 \rangle - \langle I \rangle^2 / \langle I \rangle^2)$. Here, I denotes the signal intensity and the ensemble average is shown in angle brackets. S_4 normally takes fractional values between 0 and 1, and rises with scintillation intensity. Here, the S_4 index used was calculated every 10 minutes from the receiver signal of one of the three units. At a low satellite elevation angle, the signal intensity changes due to ionospheric scintillation as well as other causes. Therefore, data obtained at elevation angles exceeding 30° were used. This made it possible to observe scintillations generated on the radio wave propagation path that passes within a circle having a radius of 520 km centered at an altitude of 300 km above Kototabang (Fig. 1). This circle covers geomagnetic latitudes 4° S to 13° S. Plasma bubbles occur in the F layer on the magnetic equator and propagate eastward as the bubbles gradually develop at higher altitudes. As evident from Fig. 1, when there is a low upper-limit altitude of bubbles on the magnetic equator, the region is beyond the field of view and bubbles in that region cannot be detected.

2.2 Long-term changes and periods in scintillation generation

Figure 3 shows the temporal and daily changes in the S_4 index observed during a period of about six and a half years from the latter half of January 2003 to mid-June 2009. The vertically long black portion offers no data due to trouble with the receiving system and elsewhere. Moreover, we ignored low S4 values of about 0.2 and lower that may be due to radio wave interference, receiver noise, and other causes. From Fig. 3, we point out the following:

(1) Scintillation activity declined each year after 2003, when solar activity was declining, and remained almost still after 2007. (As described above, note that scintillations caused by bubbles other than those developing at high altitudes cannot be observed in Kototabang. Therefore, Fig. 3 may not correctly reflect changes in bubble activity over the equator.)

(2) Scintillation activity is high from March to April and from September to October, and occurs from 20:00 to 01:00 LT (13:00 to 18:00 UT).

(3) The occurrence of scintillations changes irregularly according to the day, but is more frequent (and with higher S_4 values) in March to April than in September to October.

The characteristics above agree well with those of plasma bubbles near longitude 100° E as observed by satellite (see [15]). Plasma bubbles photographed by an all-sky camera or similar optical equipment are known to exist from after sunset until more than a few hours after midnight. The reason why scintillation only occurs until around midnight is presumably because electron density irregularities of the 350 nm scale disappear around midnight. The results of Fig. 3 strongly suggest that the characteristics of bubble activity from after

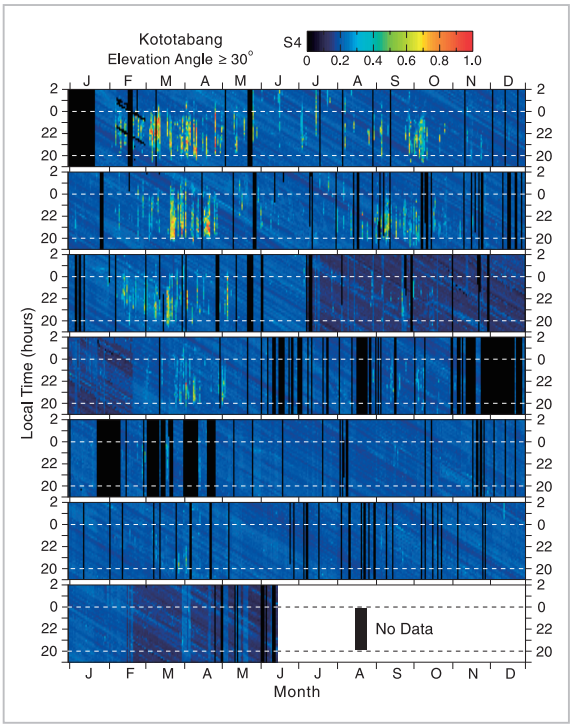

Fig.3 *Temporal and daily changes in the S_4 index from late January 2003 to mid-June 2009*

No measurements were made for the black region.

sunset to midnight over Kototabang can be clarified from GPS scintillation observation.

As described above, scintillations (therefore, plasma bubbles) occur irregularly according to the day. In order to examine whether scintillation occurs quite irregularly or with some regularity, long-term S_4 data are subjected to wavelet analysis. Figure 4 shows, for 920 days from January 1, 2003 to July 10, 2005, (a) temporal and daily changes in S_4, (b) daily changes in S_4 deviation (calculated by averaging S_4 obtained from 18:00 to 02:00 LT on each day during 920 days, and subtracting this from the average between 18:00 and 02:00 LT on each day), and (c) the results obtained by subjecting these changes in deviation to wavelet analysis. Figure 4 (b) is marked with the date of storm commencement (SC). Although several geomagnetic storms may have induced scintillations, no clear correlation is seen between scintillations and the onset of geomagnetic storms in the spring and autumn. From Fig. 4 (c), although several spectral peaks are seen between periods of 2 to 30 days in the spring and autumn, these peaks are presumably due to planetary-scale atmospheric waves (PW) and solar activity.

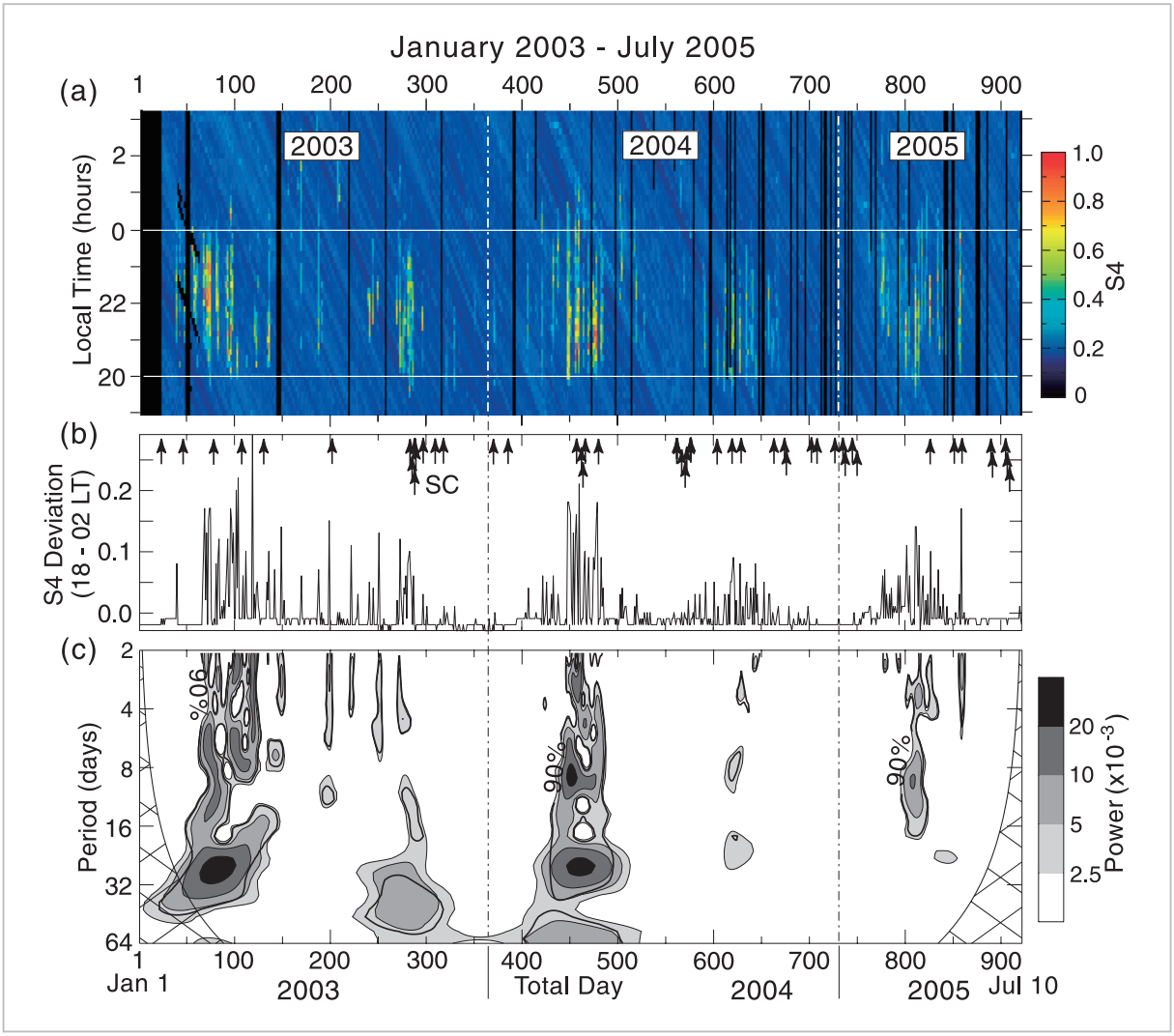

Fig.4 *(a) Temporal and daily changes in S_4 from January 1, 2003 to July 10, 2005 (b) Daily changes in S_4 deviation (obtained by averaging S_4 from 18:00 to 02:00 LT during the same period, and subtracting this from the average of 18:00 to 02:00 LT on each day) (c) Wavelet analysis of S_4 deviation. The thick-line curve represents a 90% confidence level. The cross-hatched portion is unreliable* [13]

3 Relation between GPS scintillation and tropospheric convection

The preceding chapter suggested that upward-propagating PW generated from tropospheric disturbance are related to the generation of equatorial GPS scintillation. This chapter examines this possibility in more detail. Tropospheric disturbance on the equator is caused by temporal and spatial changes in rain, clouds, atmospheric pressure, convection, and other factors. The parameter used here to represent the degree of disturbance is the cloud-top temperature (T_{bb}) observed by a geostationary meteorological satellite. In general, as tropospheric convection becomes active (or inactive) for various reasons, the cloud top rises (or lowers), and T_{bb} lowers (or rises). As tropospheric convection becomes active, AGW and PW having various periods are presumably intensely excited, and then propagate upwards through the stratosphere.

Figure 5 compares the daily changes in S_4 (shown in Fig. 4) and T_{bb} during the period from March 1 to April 30, 2003. In the T_{bb} plot in the left figure, the x-axis is east longitude, with Kototabang at 100.32° E. For T_{bb}, the average between latitude 2° N to 2° S and that between 00:00 and 24:00 UT are plotted. From this figure, for example, from day 80 to day 90, a low-temperature region at not more than 250 K can be seen moving eastward over the Indian Ocean. Unlike the situation over the Indian Ocean, one reason for the irregular temperature distribution near Kototabang is presumably the effect of high mountains on the island of Sumatra. Comparing the left figure with the right figure shows that scintillation also occurs not only when T_{bb} is low over the Indian Ocean (with high cloud top) but also when it is high (with low cloud top), thereby suggesting that some kind of tropospheric disturbance contributes to the generation of scintillation. For a detailed discussion of the correlation between T_{bb} and S_4 over the

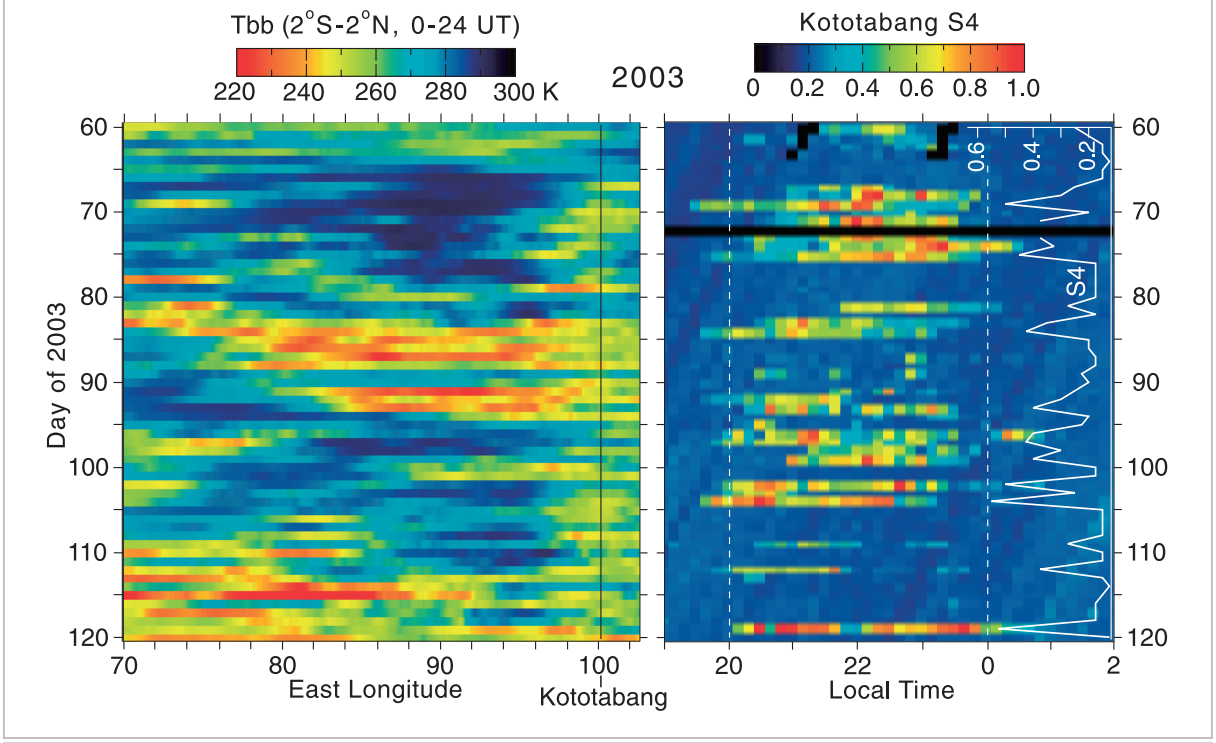

Fig.5 *(Left) Longitudinal and daily changes in T_{bb} averaged between 2°N and 2°S, and between 00:00 and 24:00 UT from March 1 (day 60) to April 30 (day 120), 2003 (Right) Temporal and daily changes in the S_4 index during the same period. The white-line curve represents daily changes in S_4 averaged between 18:00 and 02:00 LT.* [13]

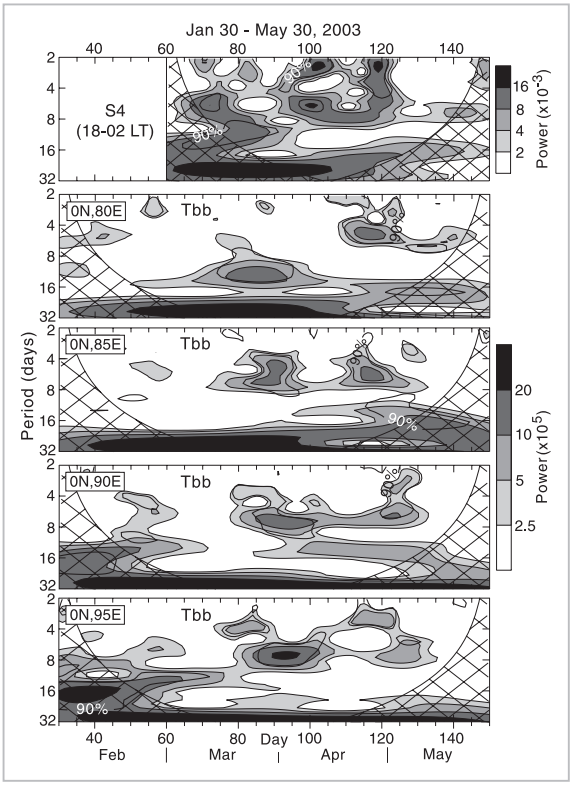

Fig.6 *Wavelet analyses of S_4 deviation (see Fig. 4 (c)) and T_{bb} at four points on the equator*

The thick-line curve represents a 90% confidence level. The cross-hatched portion is unreliable.

Indian Ocean, refer to Ogawa et al.[9][13].

Long-term changes in the S_4 wavelet spectrum were shown in Fig. 4. Here we note the period from February to May 2003 and compare the wavelet spectrum of S_4 and T_{bb}. The top row in Fig. 6 shows the S_4 spectrum during this period and the bottom row indicates the T_{bb} spectra at four points (80° , 85° , 90° and 95° E) over the equator (0° N). The T_{bb} spectra at the different points show several peaks having periods of 3 to 16 days, and corresponding peaks are also seen in the S_4 spectrum. Figure 7 shows the spectral intensity of S_4 and T_{bb} obtained from Fig. 6. The T_{bb} peaks are near the periods of 5, 7, and 14 days, as are the S_4 peaks. However, the peaks near the periods of 2 to 3 days and 25 days seen in S_4 are not present in T_{bb}. As a result, Figs. 6 and 7 suggest that PW from the troposphere having periods longer than 5 days contribute to the generation of scintillations. The periods of PW called normal mode Rossby waves are 2, 5, 10, and 16 days[16], and several periods indicated above are close to these periods.

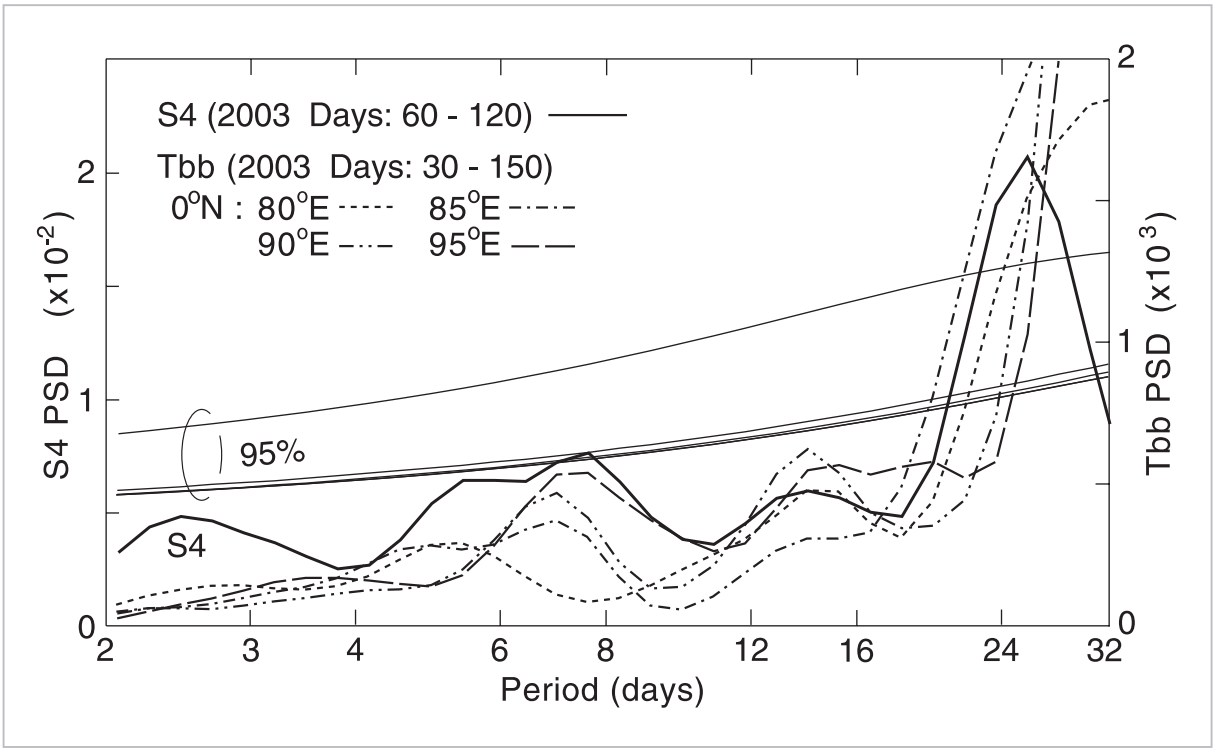

Fig.7 *Periodgram (period versus spectral density) of S_4 deviation and T_{bb} obtained from Fig. 6*

The smooth curve represents a 95% confidence level.

4 Numerical simulation of atmospheric waves

The preceding chapter (based on an analysis of S_4 and T_{bb} data) indicated the possibility of long-period atmospheric waves from the bottom layer controlling the generation of scintillations (plasma bubbles). However, it is very difficult to prove from scintillation observations and other observation methods of the ionosphere and thermosphere alone that these atmospheric waves exist at thermospheric and ionospheric altitudes. Here, the Kyushu University General Circulation Model (KUGCM) developed by Kyushu University was used to conduct numerical simulations intended to study the behavior of equatorial atmospheric waves, thereby examining what kind of waves can exist in the thermosphere. For details of the KUGCM, refer to other documents (see[17][18]). Because east-west neutral winds are important for the generation of bubbles (see[19]), only the east-west winds are examined here.

Figure 8 (a) shows the frequency spectra of east-west winds at altitudes of 90, 100, 150, and 200 km as calculated from simulation data for one year and obtained at certain points near the equator (0.4° N, 100° E), and Fig. 8 (b) shows those obtained during the last 10 days of March; Fig. 8 (a) plots spectra with

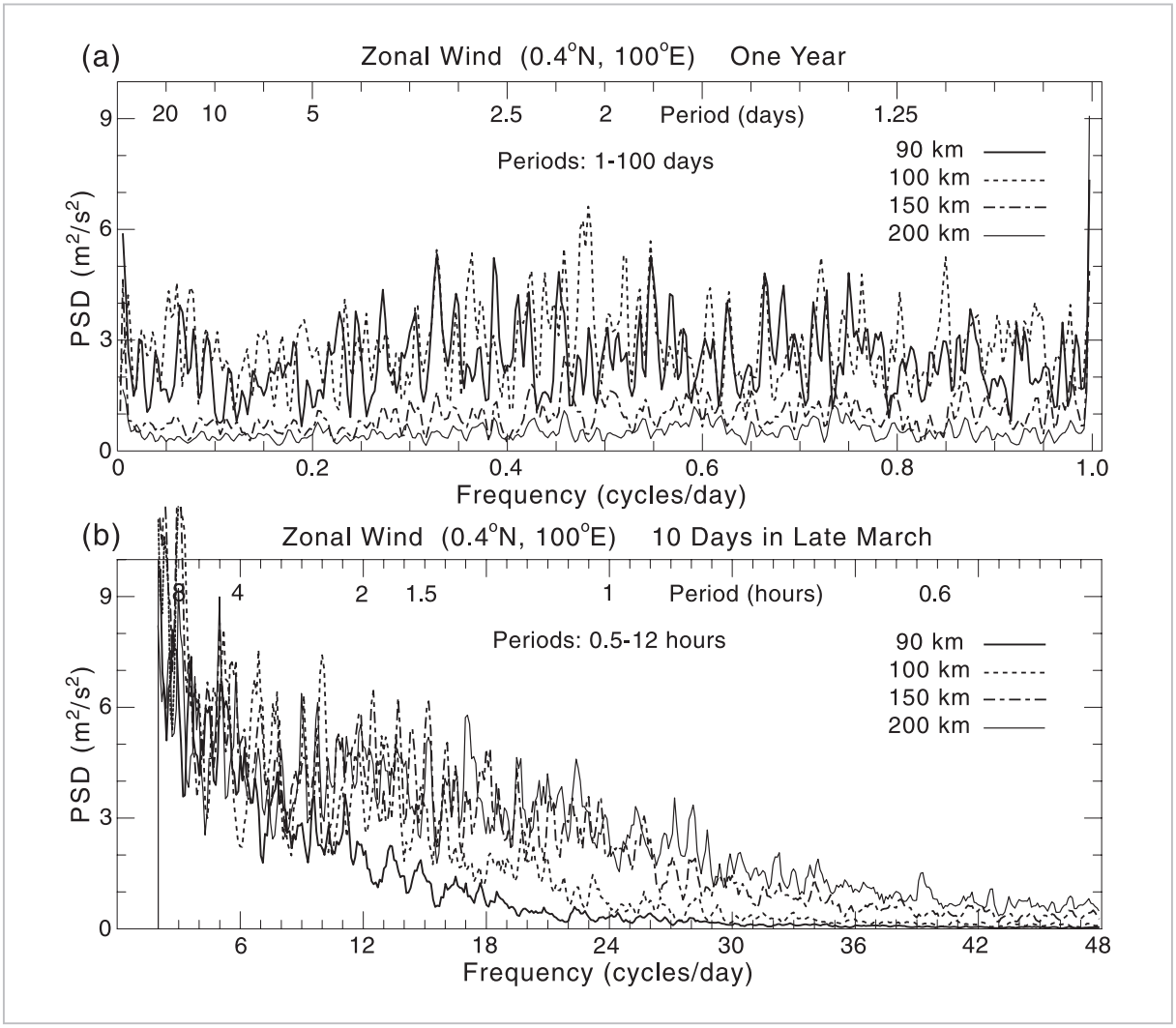

Fig.8 *Frequency spectra of east-west winds near Kototabang as obtained from numerical simulation data throughout the year and during the last ten days of March*[13]

(a) Periods of 1 to 100 days, (b) periods of 0.5 to 12 hours. Given the very high intensity, the components for one day and half a day are omitted.

periods of 1 to 100 days and Fig. 8 (b) plots those with periods of 0.5 to 12 hours. As is evident from Fig. 8 (a), waves having a period of about one day or more attenuate quickly at altitudes above 100 km, and do not exist at 150 km or higher. Conversely, the amplitudes of waves having periods of 0.5 to 3 hours (Fig. 8 (b)) increases with altitude, and the waves can propagate up to 400 km as described below. Based on the simulation data for one year obtained at 2.8° N and longitude 0° to 360° , Fig. 9 shows how the amplitudes of

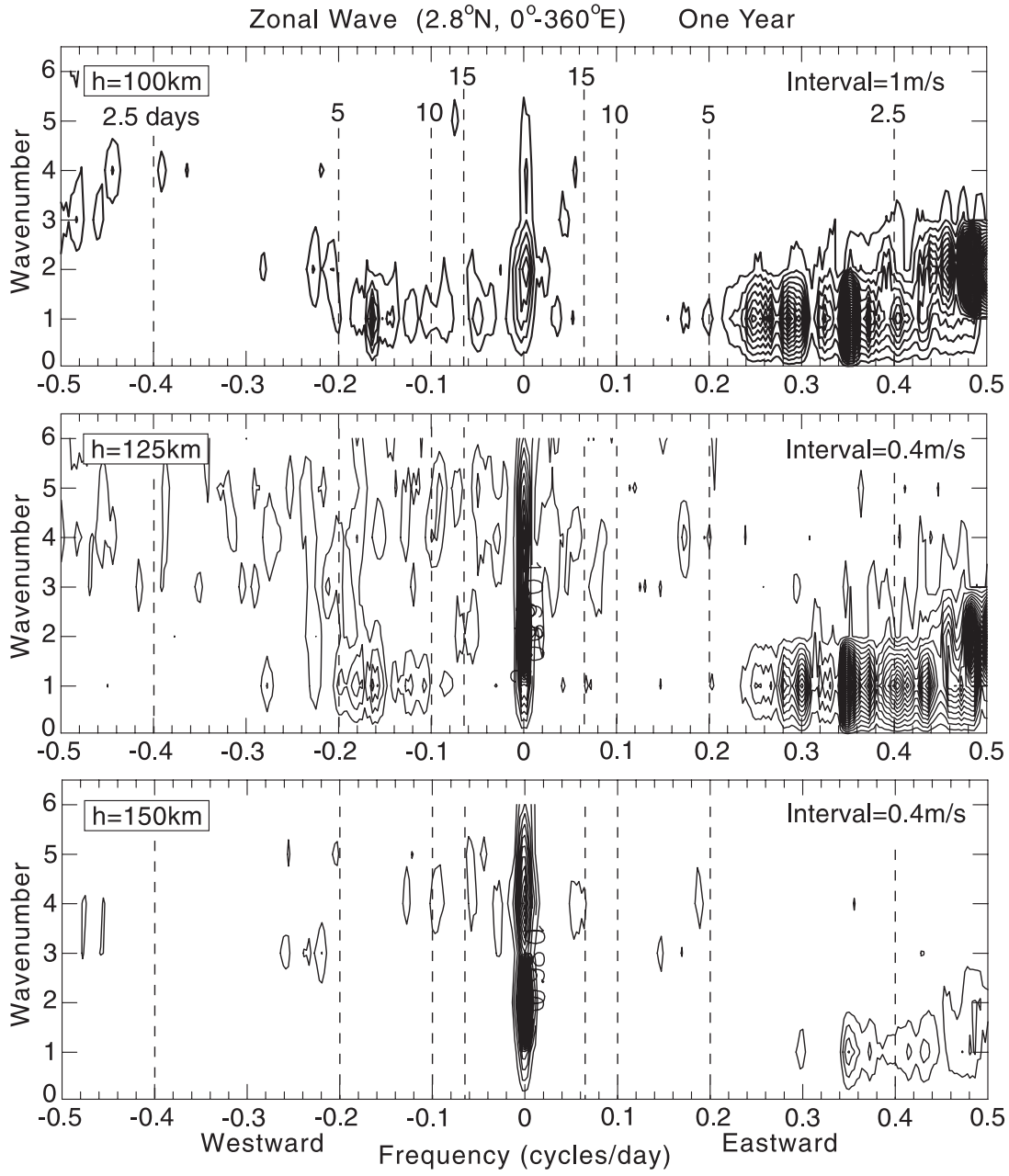

Fig.9 *Power spectra of atmospheric waves at 2.8° N having periods longer than 2 days as obtained from numerical simulation data spanning one year* [13]

The peaks near zero frequency are due to the seasonal and yearly changes in waves.

westward-propagating PW (negative frequency) having periods longer than 2 days and those of eastward-propagating Kelvin waves (positive frequency) attenuate with altitude. As described above, waves having periods of 2 to 20 days attenuate at 125 km or higher, but several wave components exist at up to 125 km. Particularly prominent are Kelvin waves having an east-west wave number (K) of 1 to 3 and a period of 2 days, and PW having a K of 1 and a period of 6 days. Other waves present include PW having a K of 2 and a period of 4 days, PW having a K of 1 and periods of 5, 10, and 16 days, and PW having a K of 3 to 4 and a period of 2 to 2.5 days. Figure 7 shows the waves having periods of 2.5, 5, 8, 14, and 25 days. These periods are partially consistent with the simulation results in Fig. 9. Moreover, it is also pointed out that PW having a periods longer than 2 days modulate the equatorial mesosphere and thermosphere [10][11].

We note that the simulation data at altitudes of 150 to 350 km in March reveal that east-west winds at altitudes above 200 km over Kototabang are eastward (with a maximum wind velocity of about 80 m/s around

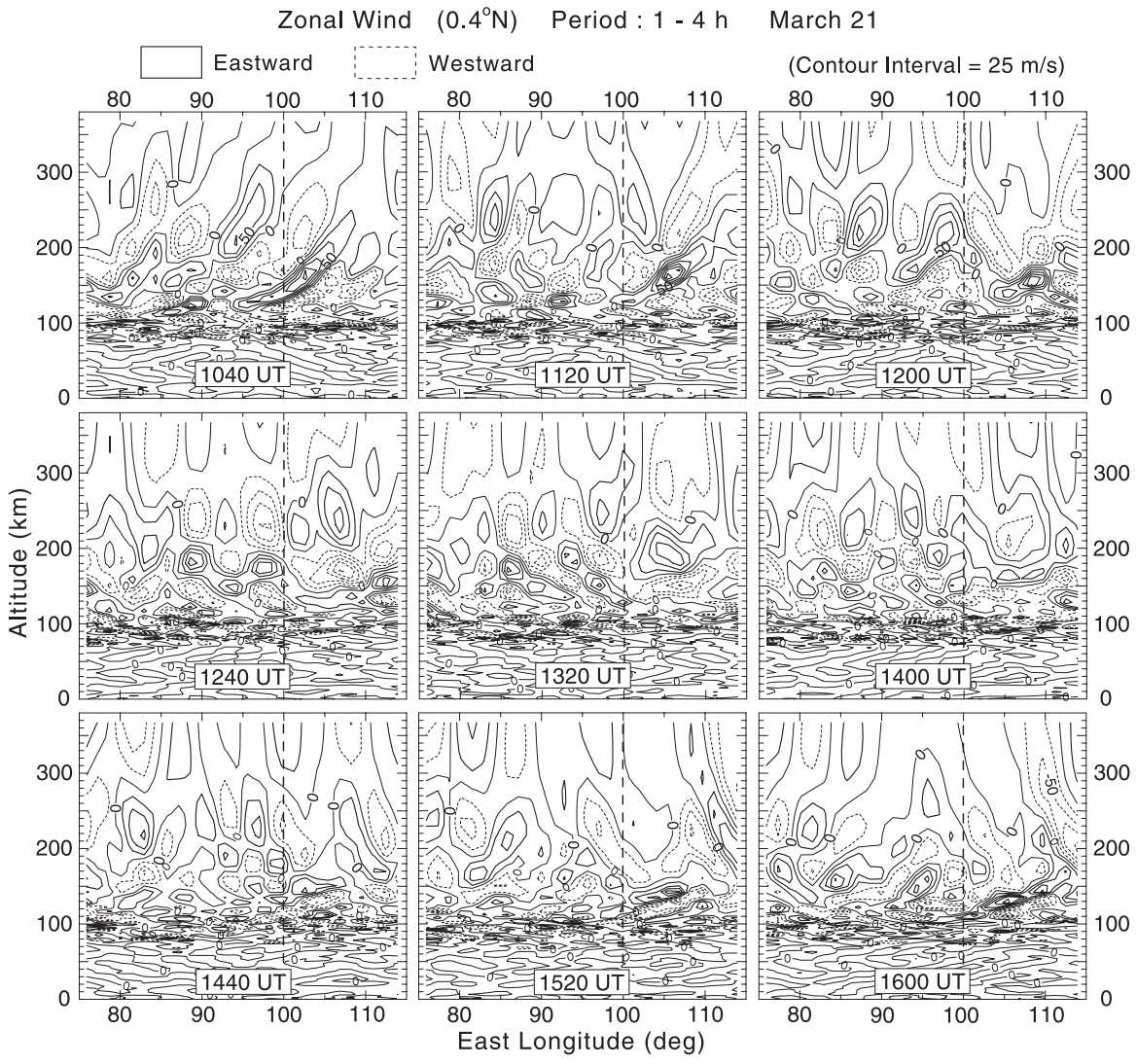

Fig. 10 *Cross section of longitudes and altitudes of east-west winds (with periods of 1 to 4 hours) every 40 minutes as obtained from numerical simulation data on March 21* [13]

The solid lines (broken lines) are eastward. The vertical broken line indicates the longitude of Kototabang.

midnight) during the nighttime from sunset to sunrise due to diurnal tide, and westward at 80 m/s maximum during the daytime [see 13 in detail]. The eastward wind at around sunset plays an important role in increasing the eastward electric field in the equatorial F layer, which triggers the generation of plasma bubbles [19].

In Fig. 8 (b), it was pointed out that the higher the altitude, the more important the short-period AGW with periods of 0.5 to 12 hours. In particular, AGW with periods of 1 to 4 hours are used to examine east-west winds that appear in the sky near Kototabang (0.4° N). Figure 10 shows the temporal changes every 40 minutes in east-west winds at 10:40 to 16:00 UT (17:40 to 23:00 LT at Kototabang) as based on simulation data from March 21. Each figure plots the contours of wind velocity by using the east longitude and altitude coordinates, with the solid lines representing eastward winds and the broken lines westward winds. At altitudes of 120 to 300 km, the regions of eastward and westward winds are both 300 to 1,000 km in the longitudinal direction, and have scales of 30 to 100 km in the altitudinal direction. Moreover, both regions generally move eastward at about 100

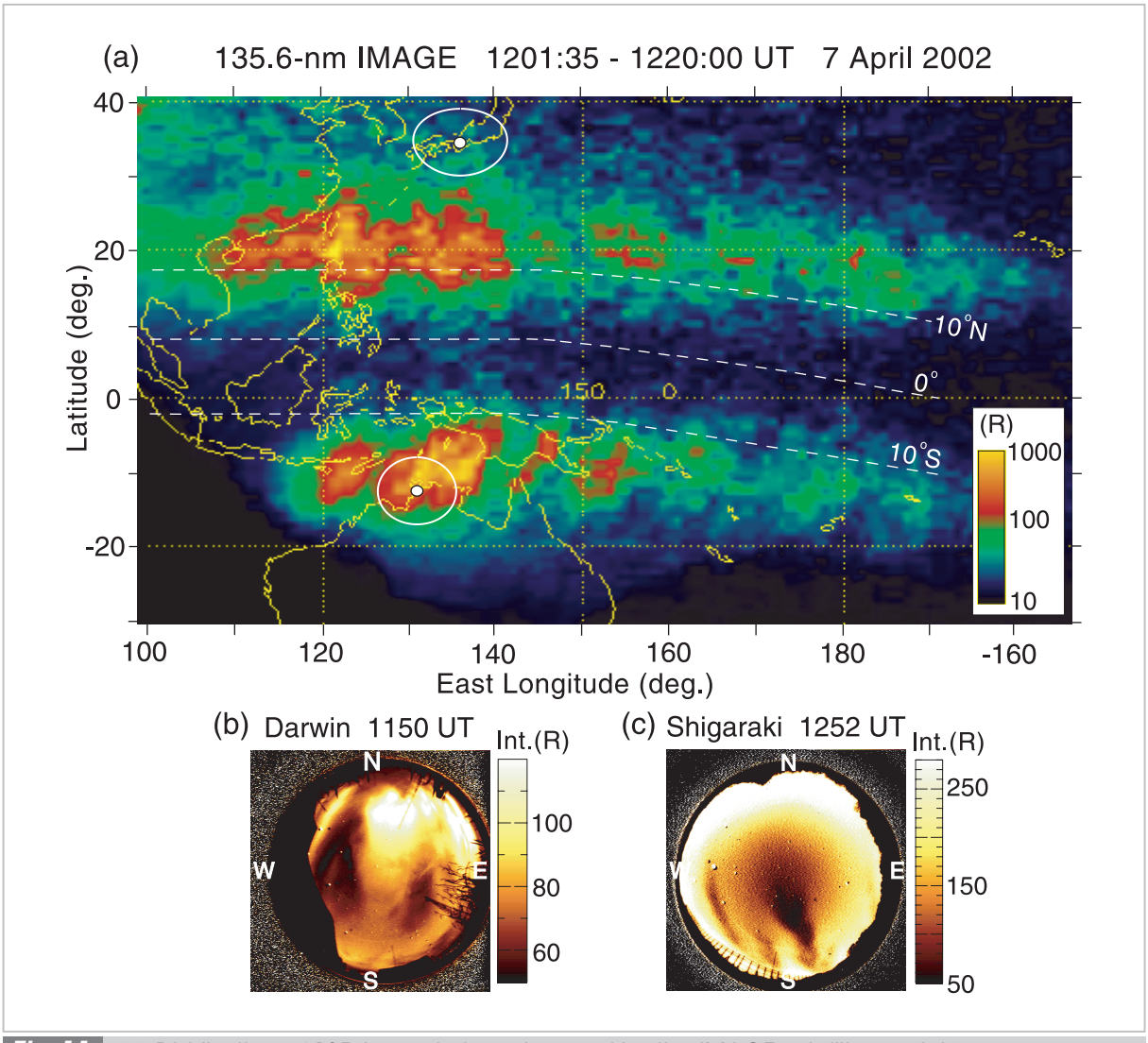

Fig.11 *(a) Distribution of 135.6 nm airglow observed by the IMAGE satellite, and (b) geomagnetic-conjugate plasma bubbles photographed by an all-sky camera at Shigaraki, Japan, and by one in (c) Darwin, Australia* [9]

The circle in white line represents the field of view of the all-sky cameras at both Shigaraki and Darwin.

m/s while changing shape, and almost agree with temporal changes in east-west winds in the sky above Kototabang as mentioned above. The wind velocity in each region also changes with time and reaches a maximum of about 100 m/s. The wave structure at altitudes of 120 km or higher (as shown in Fig. 10) is mainly due to ion drag and molecular viscosity, which also affect the upward propagation of PW in the thermosphere.

Figure 11 shows multiple geomagnetic-conjugate plasma bubbles, separated east-west between each other by 200 to 250 km, appearing within corrugated structures of F layer electron density. The structures have east-west scales of several hundred to 1,000 km and move eastward at about 100 m/s [8][9], which supports the simulation results shown in Fig. 10. As described at the beginning of this paper, many researchers have pointed out that AGW propagating through the equatorial thermosphere are related to the generation of bubbles and to wavy structure at the bottom of the F layer (see [2]-[7], [20]).

5 Summary

This paper briefly discussed equatorial ionospheric disturbances based on long-term observation of the GPS scintillation phenomenon and numerical simulation. As described at the beginning, most of the contents covered here have already been reported in journals, and the text given here is a simple review of those papers. The main results are as follows:

(1) The generation of scintillation above Kototabang is closely related to the presence of equatorial plasma bubbles, and scintillation observation is an effective means of elucidating the bubble phenomenon. Scintillation activity since 2003 has been declining with a decline in solar activity. Such activity is asymmetric between the spring and autumn. These characteristics agree with the characteristics of plasma bubbles observed, for example, by satellites.

(2) Scintillation occurs mainly between 20:00 and 01:00 LT, but its possible occurrence changes day by day. As a result of wavelet analysis of the long-term S_4 index, the generation of scintillation is found to be related to PW propagating from the bottom layer and having periods longer than 2 days. This fact is also supported by wavelet analysis of T_{bb}, an index of equatorial tropospheric disturbance.

(3) As a result of numerical simulations using the KUGCM to determine the characteristics of atmospheric waves in the thermosphere near the equator, it is found that long-period PW and Kelvin waves do not propagate to an altitude higher than 120 km, but short-period AGW exist even at altitudes higher than 120 km. AGW form a structure of east-west winds having a scale of 100 to 1,000 km and moving eastward at about 100 m/s. The behavior of such east-west winds is presumably closely related to the generation of bubbles around sunset and their eastward movement after generation.

(4) As described above, PW and Kelvin waves cannot propagate to altitudes where bubbles are present. Supposing that electrical fields generated at altitudes of the E layer by these atmospheric waves are transported to altitudes of the F layer along the geomagnetic field line, the effect of PW and Kelvin waves appears in scintillation activity (bubbles).

As such, it is considered beyond doubt that AGW and PW propagating from the bottom layer are related to the electrodynamic process of the equatorial ionosphere, but more research is needed regarding the detailed interaction process between neutral atmospheric waves and plasma, and for elucidating the triggering process in bubble generation by AGW, along with other issues. Moreover, it will become important in the future to conduct simulations that fuse the neutral atmosphere

with the plasma process.

Last but not least, the author thanks Dr. Yuichi Otsuka (Solar-Terrestrial Environment Laboratory, Nagoya University) for providing the latest data about GPS scintillation, and Dr. Yasunobu Miyoshi (Department of Earth and Planetary Sciences, Kyushu University) for offering simulation data. The author wishes to acknowledge both persons for their valuable assistance.

References

1 M. A. Abdu, "Outstanding Problems in the Equatorial Ionosphere-Thermosphere Electrodynamics Relevant to Spread F," Journal of Atmospheric and Solar-Terrestrial Physics, Vol. 63, pp. 869–884, 2001.

2 J. Röttger, "Travelling Disturbances in the Equatorial Ionosphere and Their Association with Penetrative Cumulus Convection," Journal of Atmospheric and Solar-Terrestrial Physics, Vol. 39, pp. 987–998, 1977.

3 J. Rötger, "Equatorial Spread-F by Electric Fields and Atmospheric Gravity Waves Generated by Thunderstorms," Journal of Atmospheric and Solar-Terrestrial Physics, Vol. 43, pp. 453–462, 1981.

4 M. C. Kelley, M. F. Larsen, C. LaHoz, and J. P. McClure, "Gravity Wave Initiation of Equatorial Spread F: A Case Study," Journal of Geophysical Research, Vol. 86, pp. 9087–9100, 1981.

5 S. Singh, F. S. Johnson, and R. A. Power, "Gravity Wave Seeding of Equatorial Plasma Bubbles," Journal of Geophysical Research, Vol. 112, pp. 7399–7410, 1997.

6 C. S. Lin, T. J. Immel, H. C. Yeh, S. B. Mende, and J. L. Burch, "Simultaneous Observations of Equatorial Plasma Depletion by IMAGE and ROCSAT- 1 Satellites," Journal of Geophysical Research, Vol. 110, A06304, doi: 10.1029/2004JA010774, 2005.

7 R. T. Tsunoda, "On the Enigma of Day - to - Day Variability in the Equatorial Spread F," Geophysical Research Letters, Vol. 32, L08103, doi: 10.1029/2005GL022512, 2005.

8 T. Ogawa, E. Sagawa, Y. Otsuka, K. Shiokawa, T. J. Immel, S. B. Mende, and P. Wilkinson, "Simultaneous Ground- and Satellite-Based Airglow Observations of Geomagnetic Conjugate Plasma Bubbles in the Equatorial Anomaly," Earth Planets Space, Vol. 57, pp. 385–392, 2005.

9 T. Ogawa, T., Y. Otsuka, K. Shiokawa, A. Saito, and M. Nishioka, "Ionospheric Disturbances Over Indonesia and Their Possible Association With Atmospheric Gravity Waves From the Troposphere," Journal of the Meteorological Society of Japan, Vol. 84A, pp. 327–342, 2006.

10 H. Takahashi, L. M. Lima, C. W. Wrasse, M. A. Abdu, I. S. Batista, D. Gobbi, R. A. Buriti, and P. P. Batista, "Evidence on 2-4 Day Oscillations of the Equatorial Ionosphere h'F and Mesospheric Airglow Emissions," Geophysical Research Letters, Vol. 32, L12102, doi: 10.1029/2004GL022318, 2005.

11 M. A. Abdu, P. P. Batista, I. S. Batista, C. G. M. Brum, A. J. Carrasco, and B. W. Reinisch, "Planetary Wave Oscillations in Mesospheric Winds, Equatorial Evening Prereversal Electric Field and Spread F," Geophysical Research Letters, Vol.33, L07107, doi: 10.1029/2005GL024837, 2006.

12 J. Laštovička, "Forcing of the Ionosphere by Waves From Below," Journal of Atmospheric and Solar-Terrestrial Physics, Vol. 68, pp. 479–497, 2006.

13 T. Ogawa, T., Y. Miyoshi, Y. Otsuka, T. Nakamura, and K. Shiokawa, "Equatorial GPS Ionospheric Scintillations Over Kototabang, Indonesia and Their Relation to Atmospheric Waves From Below," Earth Planets Space, Vol. 61, pp. 397–410, 2009.

14 Y. Otsuka, Y., K. Shiokawa, and T. Ogawa, "Equatorial Ionospheric Scintillations and Zonal Irregularity Drifts Observed With Closely -Spaced GPS Receivers in Indonesia," Journal of the Meteorological Society of Japan, Vol. 84A, pp. 343–351, 2006.

15 L. C. Gentile, W. J. Burke, and F. J. Rich, "A Global Climatology for Equatorial Plasma Bubbles in the Topside Ionosphere," Annales Geophysicae, Vol. 24, pp. 163–172, 2006.

16 J. M. Forbes, "Planetary Waves in the Thermosphere - Ionosphere System," Journal of Geomagnetism and Geoelectricity, Vol. 48, pp. 91–98, 1996.
17 Y. Miyoshi and H. Fujiwara, "Excitation Mechanism of Intraseasonal Oscillation in the Equatorial Mesosphere and Lower Thermosphere," Journal of Geophysical Research, Vol. 111, D14108, doi: 10.1029/2005JD006993, 2006.
18 Y. Miyoshi and H. Fujiwara, "Gravity Waves in the Thermosphere Simulated by a General Circulation Model," Journal of Geophysical Research, Vol. 113, D01101, doi: 10.1029/2007JD008874, 2008.
19 D. T. Farley, E. Bonelli, B. G. Fejer, and M. F. Larsen, "The Prereversal of the Zonal Electric Field in the Equatorial Ionosphere," Journal of Geophysical Research, Vol. 91, pp. 13,723–13,728, 1986.
20 S. Prakash, "Production of Electric Field Perturbations by Gravity Wave Winds in the E Region Suitable for Initiating Equatorial Spread F," Journal of Geophysical Research, Vol. 104, pp. 10,051–10,069, 1999.

***OGAWA Tadahiko**, Dr. Eng.*
Guest Researcher, Environment Sensing and Network Group, Applied Electromagnetic Research Center
Upper Atmosphere Physics